Transient and Time-Resolved Resonance Raman Investigation of Photoinitiated Electron Transfer in Ruthenated Cytochromes *c*†

M. C. Simpson,‡,§ F. Millett,|| L. P. Pan,|| R. W. Larsen,⊥ J. D. Hobbs,‡,§ B. Fan,‡ and M. R. Ondrias*,‡

Department of Chemistry, University of New Mexico, Albuquerque, New Mexico, Department of Chemistry, University of Arkansas, Fayetteville, Arkansas, and Department of Chemistry, University of Hawaii, Honolulu, Hawaii

Received February 1, 1996; Revised Manuscript Received May 13, 1996⊗

ABSTRACT: Ruthenation of exterior amino acid residues of heme proteins provides an effective means by which biological ET reactions can be studied within the context of highly complex protein environments. Resonance Raman spectroscopy can probe both ET kinetics and structural dynamics at the molecular level. Here we present the first comprehensive use of time-resolved and transient resonance Raman spectroscopies to examine photoinduced ET in cytochromes. Two ruthenated cytochromes *c*, Ru(lys72)-cyt.c and Ru(cyt102)cyt.c, were studied with TRRS using 10 ns laser pulses and with TRRRS on a 10 ns to 10 ms time scale. It was found that resonance Raman protocols can effectively trace ET kinetics and associated heme−protein structural dynamics. Care must be exercised, however, when drawing comparisons to measurements made by other methods (i.e., transient absorbance). The TRRS studies directly probe the heme and its local environment and reveal that the heme dynamics accompanying ET are very rapid relative to phenomenological ET kinetics. The heme and its local environment evolve to their equilibrium (ferrous) structure in less than 10 ns subsequent to ET, with no evidence for the existence of metastable heme pocket geometries analogous to those observed in the dynamic response of hemoglobins and oxidases. Finally, species-specific differences are observed in the photoinduced ET kinetics and heme structural dynamics. However, these differences are confined to nanosecond or faster time scales.

Metalloporphyrin (MP)-mediated electron transfer (ET)[1] reactions play major roles in the metabolic pathways of virtually all living organisms. In plants and photosynthetic bacteria, the conversion of sunlight into useful forms of energy involves ET between chlorophylls and pheophytins in the photosynthetic reaction center. In animals, the mitochondrial ET chain ultimately leads to ATP generation through a series of ET steps between MP-containing protein centers. Despite decades of intense research activity, defining the molecular bases for the specificity and rates of ET within redox active proteins remains a fundamental challenge in biophysics.

Biological ET reactions are complicated and therefore difficult to study *in situ*. ET must occur over relatively long distances and through the highly non-uniform polypeptide environment of both donor and acceptor proteins [see Moser et al. (1995) and references therein]. Also, the influence of the protein on the static and dynamic ET behavior of MP active sites is largely uncharacterized. One strategy by which many of these issues have been addressed is to attach a photoactive redox center to the surface of an isolated ET protein. Ruthenium (Ru) complexes often are used as photoactive modifying agents. Ruthenium trisbipyridine ($Ru(Py_2)_3$) derivatives can be covalently attached to externally accessible amino acids including lysine, histidine, and cysteine [see Winkler and Gray (1992), Cusanovich (1991), McLendon (1988), and Bjerrum et al. (1995) for reviews]. Photoexcitation of these derivatives creates a long lived triplet state that can donate or accept electrons (Cherry & Henderson, 1984) from the heme group. ET between the Ru at the protein surface and the heme embedded in the protein can thus be photoinitiated in well-defined manner. Cytochromes *c* are commonly studied because they are soluble, easily purified, and contain a single, well-characterized heme group. In addition, both yeast and horse heart species have well-known crystal structures (Louie et al., 1988; Bushnell et al., 1990).

Both the driving force and the donor−acceptor separation can be measured and systematically tuned in Ru−cytochrome systems (Winkler & Gray, 1992; Bjerrum et al., 1995; Durham et al., 1991; Geren et al., 1991; Winkler et al., 1982; Pan et al., 1988.) By changing the metal center in the heme and/or the coordination state of the Ru, the thermodynamic driving force ΔG can be altered while maintaining a constant donor−acceptor distance and intervening protein medium. Alternatively, attachment of the same Ru group to different amino acids on the protein leads to changes in the distance and environment between the donor and acceptor in the absence of variations in ΔG. Recently, site-directed mutagenesis has been employed to engineer ruthenium attachment sites at defined locations on the protein exterior (Wuttke et al., 1992; Geren et al., 1995). Flash photolysis or pulse

† This work was supported by the NIH (GM33330 to M.R.O. and GM20488 to F.M.) and by a Howard Hughes Predoctoral Fellowship (M.C.S.). M. C. Simpson was formerly M. C. Schneebeck.

* To whom correspondence should be addressed.

‡ University of New Mexico.

§ Current address: Fuel Sciences Department, Sandia National Laboratories, Albuquerque, NM.

|| University of Arkansas.

⊥ University of Hawaii.

⊗ Abstract published in *Advance ACS Abstracts,* July 15, 1996.

[1] Abbreviations: ET, electron transfer; RRS, resonance Raman spectroscopy; TRRS, transient resonance Raman spectroscopy; TRRRS, time-resolved transient resonance Raman spectroscopy; Ru(lys72)cyt.c, horse heart cytochrome *c* ruthenated at residue lysine 72; Ru(cys102)-cyt.c, yeast cytochrome *c* ruthenated at residue cysteine 102; MP, metalloporphyrin; SAC, sacrificial donor; λ_i, inner sphere reorganization energy; λ_o, outer sphere reorganization energy.

S0006-2960(96)00253-X CCC: $12.00

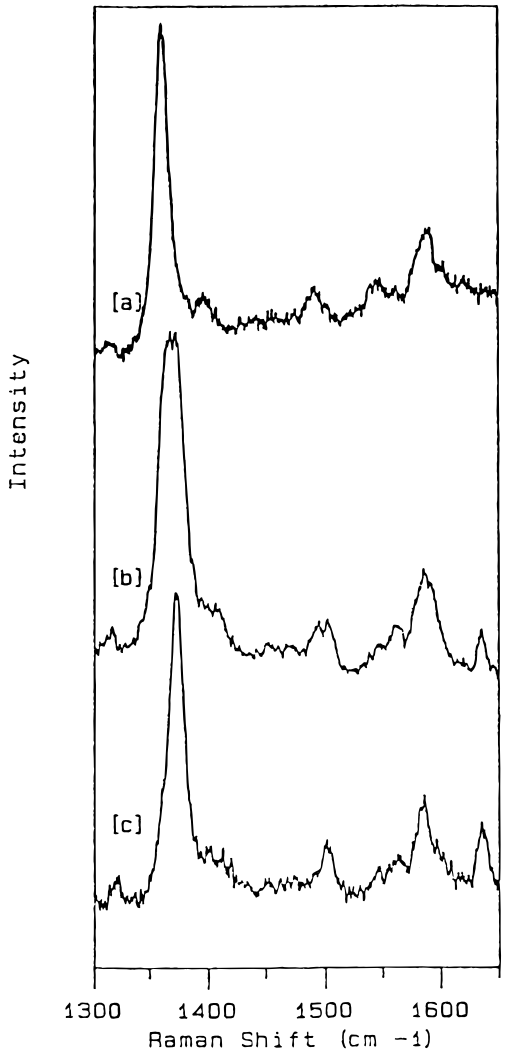

FIGURE 1: Transient resonance Raman spectra of Ru(lys72)cyt.c (~100 μM in 0.1 M Tris, pH 8.0) in the high-frequency region. Spectra were obtained with 406 nm excitation pulses of 10 ns duration and 15 Hz repetition rate. (a) Equilibrium chemically reduced species obtained with low-excitation flux ($<1 \times 10^8$ W/cm^2); (b) transient photoinduced reduction of fully oxidized species obtained with high-excitation flux (approximately 1×10^8 W/cm^2); (c) equilibrium fully oxidized species obtained with low-excitation flux.

radiolysis is generally used to initiate ET, and the progress of the ET reaction may be followed with luminescence and absorbance spectroscopies, NMR, and electrochemical methods. Studies of the distance and driving force dependence of ET have been carried out upon Ru-modified proteins, including cytochrome *c*, and the behavior of these systems has been found to be fairly consistent with traditional Marcus theory (Bjerrum et al., 1995; Winkler & Gray, 1992; Cusanovich, 1991; McLendon, 1988; Marcus & Sutin, 1985; Marcus, 1956, 1964, 1965).

Our present study expands the physical characterization of the ET dynamics of cytochromes *c* by using time-resolved (TRRRS) and transient (TRRS) resonance Raman spectroscopy to examine the vibrational structure of the heme active sites during and immediately subsequent to photoinitiated ET in two different ruthenated cytochromes. We find that the kinetics and the structural dynamics at the heme associated with ET depend upon both the ruthenated protein species in question and the experimental protocols employed.

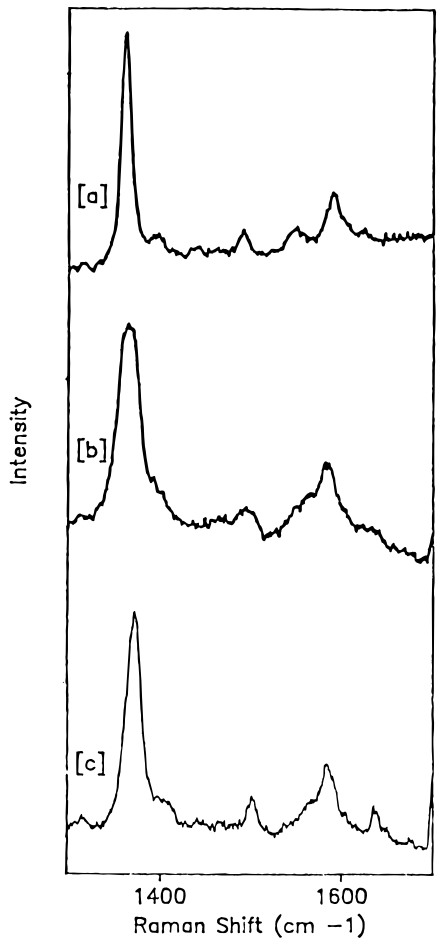

FIGURE 2: Transient resonance Raman spectra of Ru(cys102)cyt.c (~100 μM in 0.1 M Tris, pH 8.0, plus trace of cytochrome *c* oxidase) in the high-frequency region. (a) Equilibrium chemically reduced species (low-excitation flux); (b) transient photoinduced reduction of fully oxidized species (high-excitation flux); (c) equilibrium fully oxidized species (low-excitation flux). Spectroscopic conditions were the same as for Figure 1.

The observed structural responses to ET are described in the context of the well-studied dynamic behavior of hemoglobins and oxidases.

MATERIALS AND METHODS

The yeast cytochrome *c* labeled with Ru(bpy)$_2$(methylbipyridine) at cysteine 102 (Ru(cys102)cyt.c) was synthesized and purified as described by Geren et al. (1991). Horse heart cytochrome *c* labeled with Ru(bpy)$_2$(decarboxybipyridine) at lysine 72 (Ru(lys72)cyt.c) was synthesized and purified as described by Pan et al. (1988). All transient and time-resolved resonance Raman experiments were carried out under aerobic conditions. Spectra of the fully oxidized species at equilibrium were also taken under aerobic conditions with sample concentrations of 50−100 μM. Spectra of the equilibrium fully reduced derivatives were obtained from buffered samples reduced by the anaerobic addition of a slight excess of sodium dithionite. Trace amounts of beef heart cytochrome *c* oxidase were added to yeast cytochrome *c* samples in order to ensure proper reoxidation of the ferrous species (Simpson et al., 1995). See figure captions for other details.

Nanosecond transient and time-resolved Raman spectra were measured as described elsewhere (Simpson, 1994;

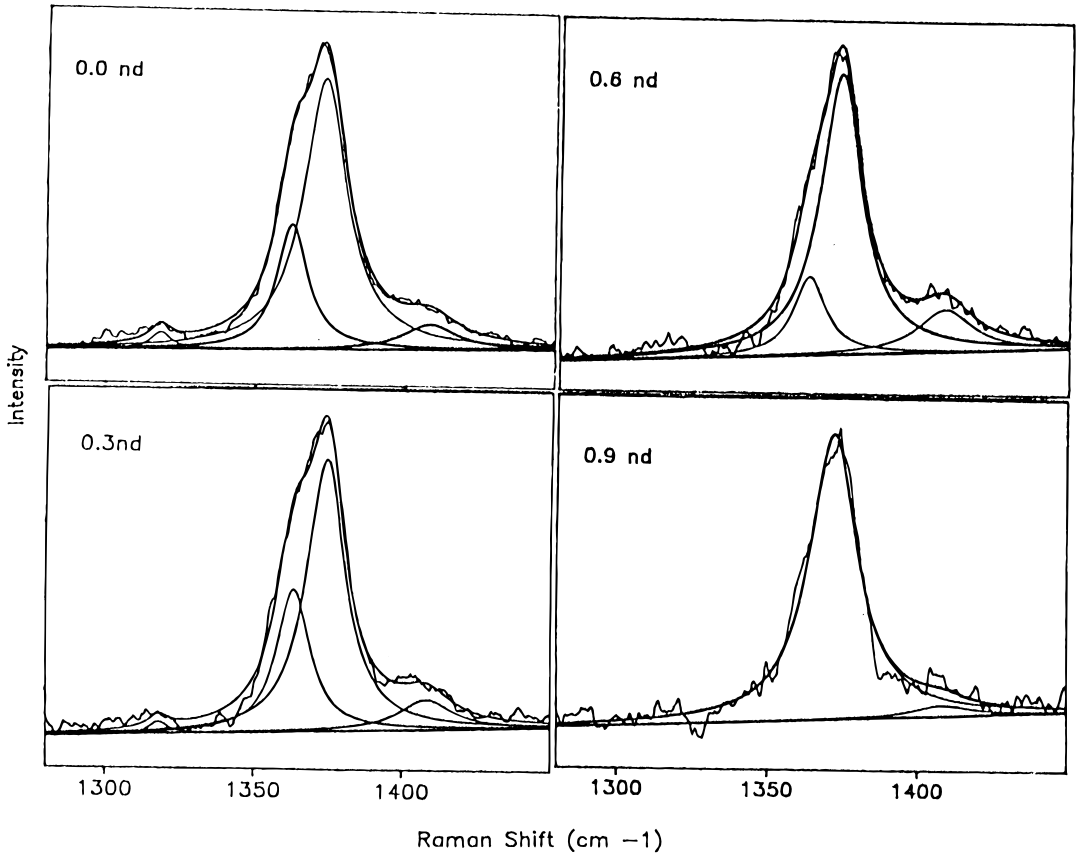

FIGURE 3: Transient resonance Raman spectra of Ru(lys72)cyt.c in the ν_4 region as a function of incident laser flux ($\lambda_{ex} = 406$ nm). All spectra were taken using a well-focused spherical lens (flux without neutral density filter, $\sim 10^8$ W/cm^2). Neutral density (nd) filters with optical densities of 0.0, 0.3, 0.6, and 0.9 (as denoted in each panel) were used to attenuate the beam. Deconvolution results are summarized in Table 1, and sample conditions were the same as in Figure 1.

Findsen & Ondrias, 1988). The incident wavelength for transient experiments was 406 nm. For time-resolved experiments involving Ru(cys102)cyt.c, the probe wavelength was 404 nm, and the pump wavelength was 450 nm. For time-resolved experiments involving Ru(lys72)cyt.c, the probe pulses were tuned to 406 nm, and the pump pulses were tuned to 355 nm. Incident laser flux was attenuated by using neutral density filters and/or focusing optics. Transient and time-resolved resonance Raman spectra were taken with 15 and 10 Hz repetition rates, respectively. Spectra were fit as described in Appendix 2.

Control measurements were made in order to ensure that pulse-to-pulse accumulation of intermediates and products did not occur and that the intrinsic photoreduction that has been observed in cytochromes *c* by others using significantly higher incident laser fluxes was not contaminating our results. In the transient experiments, the sample was exposed to different flux conditions in a random order (i.e., not in order of descending or ascending flux). The lowest flux data was collected several times during a given series of measurements. In addition, fully oxidized and fully reduced (dithionite) *unlabeled* yeast and horse heart cytochromes *c* were exposed to the high- and low-flux conditions, and no evidence of photoreduction was observed. In the TRRR experiments, the probe-only case also was measured several times throughout the series. We are confident, therefore, that the $Ru(bpy)_3$ moiety is the electron donor in our experiments and that intrinsic photoreduction is not contaminating our results.

Table 1: Transient Resonance Raman Spectral of Ru(lys72) Cytochrome *c* Characteristics of ν_4[a]

	position (cm^{-1})		width (cm^{-1})		area (%)	
experimental condition	band I	band II	band I	band II	band I	band II
no neutral density	1362	1373	13	18	25	75
neutral density filter						
+0.3 OD	1363	1374	14	16	30	70
+0.6 OD	1363	1373	13*	17	20	80
+0.9 OD	−	1372	−	19	−	100
cylindrical lens	−	1374	−	16	−	100
equilibrium fully reduced						
low flux	1362	−	12	−	100	−
high flux	1361	−	13	−	100	−

[a] Spectral characteristics of transient resonance Raman spectra of Ru(lys72)cyt.c in the ν_4 region ($\lambda_{ex} = 406$ nm). These values are results of deconvoluting the spectra in Figures 1 and 3 and other spectral data not shown.

RESULTS

Transient Resonance Raman (TRR) Studies. TRR spectra in the high-frequency region were obtained from samples of Ru(lys72)cyt.c and Ru(cys102)cyt.c. In this protocol, a single train of ~10 ns pulses ($\lambda = 406$ nm) is used to both excite the sample and generate the resonance Raman spectrum. The spectra contain contributions from all species (excited and ground states) present within the temporal extent of the excitation pulses. Figures 1 and 2 depict the high-frequency spectra obtained from the ferric and ferrous forms of these modified proteins. Low-power excitation yields spectra virtually identical to those obtained from the corre-

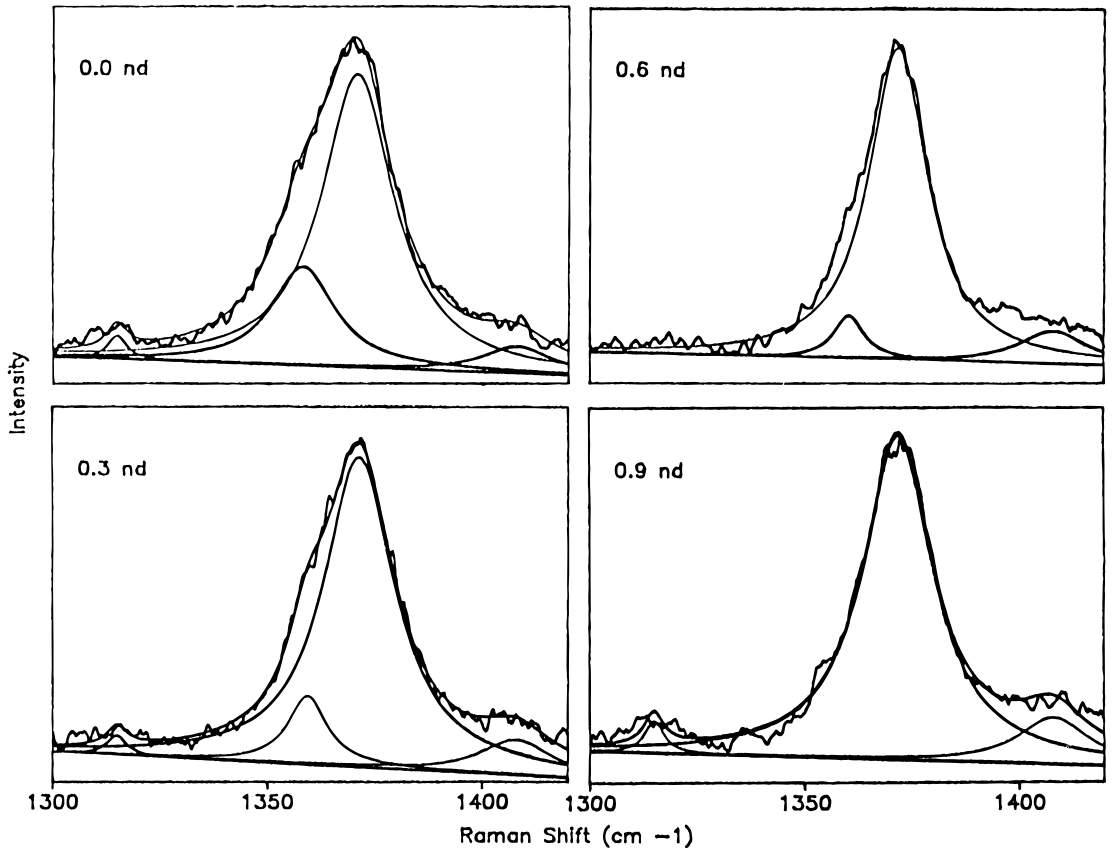

FIGURE 4: Transient resonance Raman spectra of Ru(cys102)cyt.c in the ν_4 region as a function of incident laser flux (λ_{ex} = 406 nm). All spectra were taken using a well-focused spherical lens (flux without neutral density filter, $\sim 10^8$ W/cm^2). Neutral density (nd) filters with optical densities of 0.0, 0.3, 0.6, and 0.9 (as denoted in each panel) were used to attenuate the beam. Deconvolution results are summarized in Table 2, and sample conditions were the same as in Figure 2.

sponding unlabeled, native proteins under similar conditions. This result indicates that ruthenation at the protein surface produces no major structural perturbations in the heme pocket of either horse heart or yeast cytochrome *c*.

TRR spectra obtained from the Fe^{III} heme species with high-power excitation clearly contain contributions from both ferric and ferrous hemes and thus offer direct evidence for rapid heme photoreduction in both Ru(lys) and Ru(cys) cytochromes *c*. This behavior is most evident in the oxidation state marker band ν_4, which has characteristic frequencies for ferrous and ferric heme of ~1362 and ~1374 cm^{-1}, respectively. The changes in this mode as a function of incident laser flux were quantified by spectral deconvolution.

Figure 3 and Table 1 summarize the flux-dependent response of the ν_4 band of oxidized Ru(lys72)cyt.c over an incident laser flux range of $<5 \times 10^7$ to $\sim 5 \times 10^8$ W/cm^2. Excitation with low laser intensity produces spectra with a single band at 1373 cm^{-1}, indicating a completely ferric sample. Increasing the incident beam intensity leads to the appearance of a second peak at 1362 cm^{-1}, a position characteristic of ferrous heme. ET to the heme clearly occurs within the ~10 ns laser pulse width. The relative area of the transient, ferrous ν_4 band rises with increasing laser intensity until it saturates at ~30% of the total area. The line widths and positions of the ferric and ferrous ν_4 bands are insensitive to incident laser flux (see Table 1), and the observed ET is reversible on an ~100 ms time scale, as no pulse-to-pulse accumulation of the reduced species is observed.

Table 2: Transient Resonance Raman Spectral of Ru(cys102) Cytochrome *c* Characteristics of ν_4[a]

	position (cm^{-1})		width (cm^{-1})		area (%)	
experimental condition	band I	band II	band I	band II	band I	band II
no neutral density	1358	1371	18	20	25	75
neutral density filter						
+0.3 OD	1359	1371	11	20	10	90
+0.6 OD	1360	1371	9	17	5	95
+0.9 OD	−	1372	−	20	−	100
equilibrium fully reduced	1362	−	13	−	100	−

[a] Spectral characteristics of transient resonance Raman spectra of Ru(cys102)cyt.c in the ν_4 region (λ_{ex} = 406 nm). These values are results of deconvoluting the spectra in Figures 2 and 4 and other spectral data not shown.

In a recent study (Simpson et al., 1995), we examined the power dependent behavior of the ν_4 band of ferric yeast Ru(cys102)cyt.c. Figure 4 and Table 2 are shown in order to demonstrate that the two protein systems [Ru(cys102) yeast cyt.c and Ru(lys72) horse heart cyt.c] exhibit qualitatively different behavior in our transient experiments. Specifically, there is no evidence of saturation of the ferrous ν_4 intensity at higher laser fluxes in Ru(cys102)cyt.c. Additionally, in contrast to the behavior of the Ru(lys72)cyt.c sample, the line width and position of the ferrous ν_4 band shift to lower frequency and broaden (see Table 2) as laser flux is increased (Simpson et al., 1995).

Time-Resolved Resonance Raman (TRRR) Studies. The TRRR method takes advantage of synchronized pump and probe pulse trains to first photoexcite the sample and then

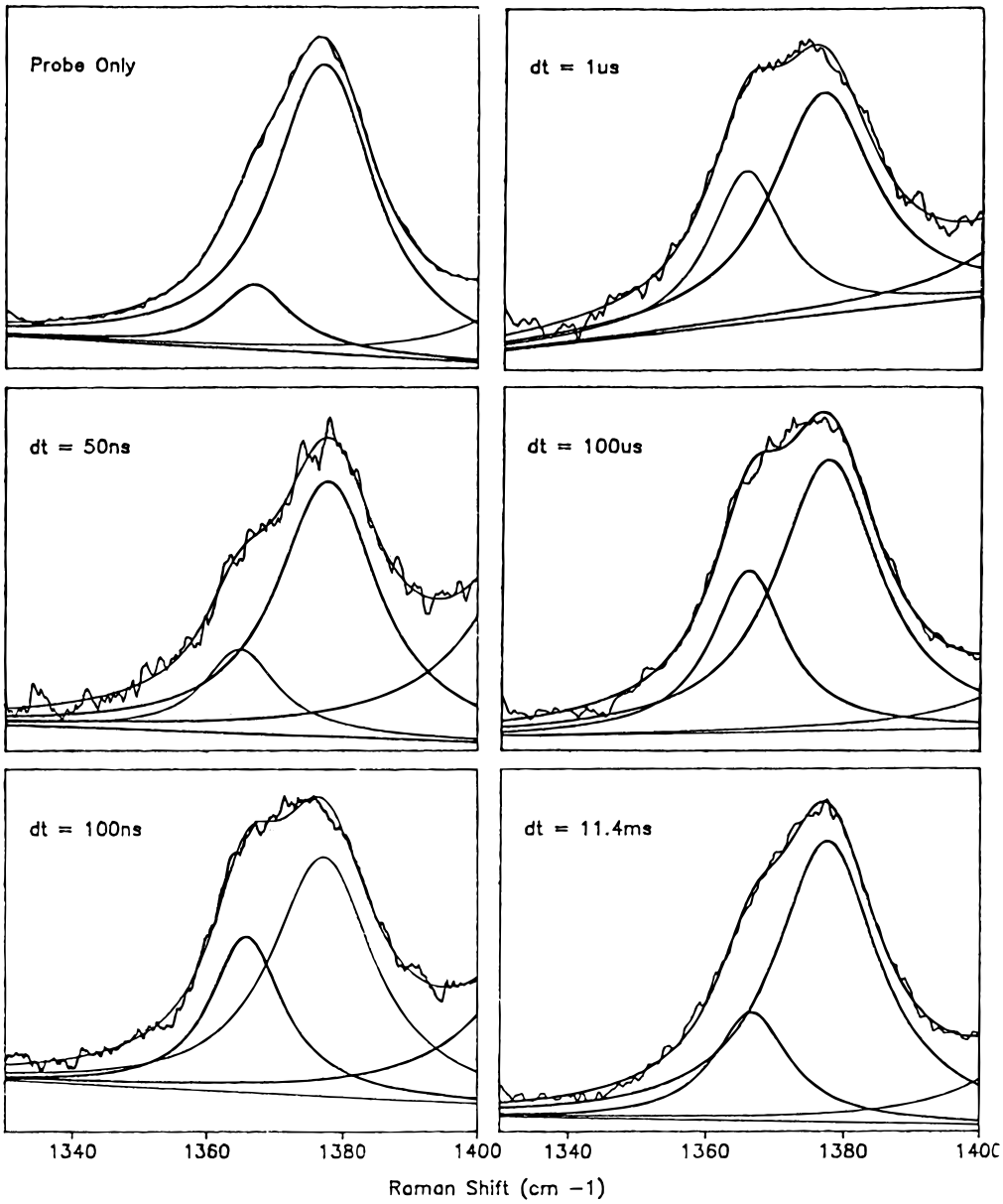

FIGURE 5: Time-resolved resonance Raman spectra of Ru(lys72)cyt.c in the ν_4 region. Pump $\lambda = 355$ nm (flux, $>10^8$ W/cm^2). Probe $\lambda = 406$ nm (flux, $<10^7$ W/cm^2). Time delay (dt) between pump and probe pulses is indicated. Results of deconvolution are summarized in Table 3, and sample conditions were the same as in Figure 1.

Table 3: Time Resolved Resonance Raman Spectral of Ru(lyx72) Cytochrome *c* Characteristics of ν_4[a]

	position (cm^{-1})		width (cm^{-1})		area (%)		corrected area[b] (%)	
experimental condition	band I	band II	band I	band II	band I	band II	band I	band II
probe only	1363	1374	13	18	14	86	–	–
$\Delta t =$								
30 ns	1632	1375	13	18	20	80	6	94
50 ns	1361	1375	13	18	19	79	6	94
100 ns	1362	1373	13	18	32	68	21	79
1.0 μs	1361	1372	13	18	33	67	22	78
10.0 μs	1362	1374	13	18	30	70	18	82
100.0 μs	1362	1373	13	18	30	70	19	81
1.4 ms	1362	1374	13	18	26	74	14	86
11.4 ms	1363	1374	13	18	22	78	9	91

[a] Spectral characteristics of time-resolved resonance Raman spectra of Ru(lys72)cyt.c in the ν_4 region. Pump $\lambda = 355$ nm. Probe $\lambda = 406$ nm. These are deconvolution results for spectra in Figure 5 and other data not shown. [b] Denotes area corrected as described in text.

monitor its temporal evolution ($\Delta t = 20$ ns to 10 ms). The TRRR spectra of Ru(lys72)cyt.c demonstrate that ET occurs on a 100 ns to 1 ms time scale in this system (Figure 5, Table 3). The spectrum in the ν_4 region obtained in the absence of the 355 nm pump beam contains two components: a band at 1362 cm^{-1} that comprises about 15% of the total intensity and a peak at 1373 cm^{-1} that makes up the other 85%. Table 3 summarizes the time-dependent

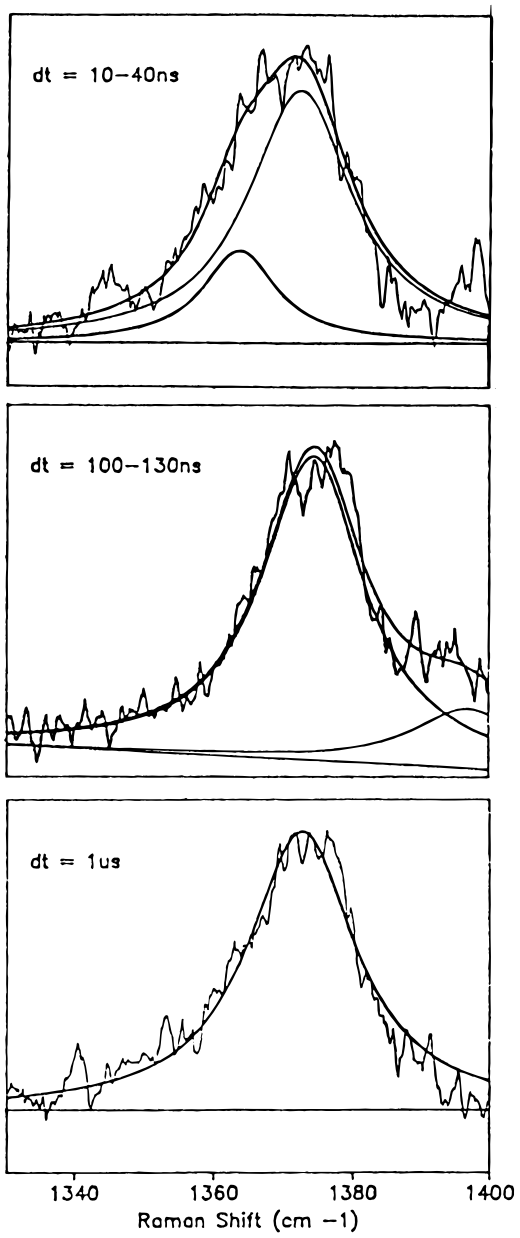

FIGURE 6: Time-resolved resonance Raman spectra of Ru(cys102)-cyt.c in the ν_4 region. Pump $\lambda = 450$ nm (flux, $\sim 10^8$ W/cm^2). Probe $\lambda = 404$ nm (flux, $<10^7$ W/cm^2). Time delay (dt) between pump and probe pulses is indicated. Results of deconvolution are summarized in Table 4, and sample conditions were the same as in Figure 2.

behavior of these vibrational transitions subsequent to excitation. When the pump precedes the probe beam by about 30 ns, the relative intensities change to become about 20% and 80%, respectively. The fraction of the 1362 cm^{-1} band increases to about 35% at 1 μs delay and then slowly decreases to 30% at 10−100 μs, 25% at 1.4 ms, and 20% at 11.4 ms. The positions of the two bands do not change significantly as a function of time. The line widths were fixed during the deconvolution procedure at equilibrium values.

TRRR spectra obtained from Ru(cys102)cyt.c with 450 nm pump pulses yielded significantly different kinetic results than did those obtained from Ru(lys72)cyt.c (Figure 6, Table 4). In the probe-only spectrum, the line was adequately fit with a single Lorentzian peak at 1373 cm^{-1}. At Δt of 10−40 ns, a second band appeared in the spectrum (1364 cm^{-1})

Table 4: Time Resolved Resonance Raman Spectral of Ru(cys102) Cytochrome *c* Characteristics of ν_4[a]

	position (cm^{-1})		width (cm^{-1})		area (%)	
experimental condition	band I	band II	band I	band II	band I	band II
probe only	−	1374	−	20	−	100
Δt =						
10−40 ns	1364	1372	13*	18*	20	80
75 ns	−	1373	−	18*	−	100
1.0 μs	−	1373	−	19	−	100

[a] Spectral characteristics of time-resolved resonance Raman spectra of Ru(cys102)cyt.c in the ν_4 region. Pump $\lambda = 450$ nm. Probe $\lambda = 404$ nm. These are deconvolution results for spectra in Figure 6 and other data not shown. [b] These linewidths were held constant.

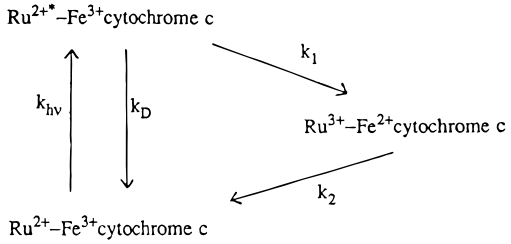

FIGURE 7: Proposed photoinitiated ET reaction scheme for Ru-(lys72)cyt.c and Ru(cys102)cyt.c (Geren et al., 1991; Durham et al., 1989). The measured values for the rate constants are listed in Table 5.

that comprised about 20% of the total intensity. Contrary to the behavior of the Ru(lys72)cyt.c species, in this system the photoreduced heme is rapidly reoxidized in this system. Indeed, at $\Delta t \approx 75$ ns, scattering from the transient ferrous species was no longer detectable. These results contrast markedly with the slower kinetics previously observed for this system (see Discussion below).

DISCUSSION

Characterization of Equilibrium Ru Cytochrome c. The chemical attachment of a Ru(bpy)$_3$ group to either cysteine 102 or lysine 72 does not significantly perturb the vibrational structure of the heme. The positions, line widths, and relative intensities of resonance Raman bands in the high-frequency spectra of the equilibrium reduced and oxidized forms of both of these cytochrome *c* derivatives are quite similar to those of unlabeled forms. This strongly suggests that the equilibrium local heme pocket geometry is not significantly altered by ruthenation. These results agree with those of Pan et al. (1988) and Geren et al. (1991) who examined the redox potentials and the UV/visible spectra of the same species. They found no evidence for large-scale label-induced protein rearrangement in the lysine-labeled cytochrome *c*, although the COOH terminus of the protein must rearrange somewhat in order to accommodate the Ru in the cysteine derivative. The current resonance Raman data support the conclusion that these putative surface structural changes are not propagated to the local heme environment of either protein.

Kinetics of ET in Ruthenated Cytochromes c. Both the transient and time-resolved resonance Raman experiments probe the kinetics and mechanism of the ET reaction in cytochrome *c*. A simple mechanism proposed for ET in these systems is depicted in Figure 7 (Geren et al., 1988; Durham et al., 1989). The rate constants for the reaction

Table 5: Kinetic and Electron Transfer Parameters Ru(lys72) Cytochrome *c* and Ru(cys102) Cytochrome *c*[a]

parameter	Ru(lys72)cyt.c	Ru(cys102)cyt.c
$k_1 = k_{ET}$	$(14 \pm 3) \times 10^6$ s^{-1}	$>10^5$ s^{-1}
k_2	$(24 \pm 3) \times 10^6$ s^{-1}	*b*
k_D	$(6 \pm 3) \times 10^6$ s^{-1}	*b*
D/A distance	8−16 Å	*b*
ΔG^0	0.98 eV	*b*
λ	0.44−0.5 eV; 2.4−2.1 eV	*b*

[a] Measured ET rate constants for photoinitiated ET reactions in Ru(lys72)cyt.c and Ru(cys102)cyt.c (Geren et al., 1991; Durham et al., 1989). These rate constants correspond to Figure 7. [b] Unknown.

steps have been reported for Ru(lys72)cyt.c (Durham et al., 1989) but not for Ru(cys102)cyt.c (Table 5). Given the reaction scheme in Figure 7, the following relationships can be derived (see Appendix 1). Unless otherwise stated, the rate constants discussed here are those depicted in Figure 7.

The TRR technique measures the steady-state populations of the reactants, products, and intermediates of the photoinitiated reaction. Thus steady-state approximations can be used to find

$$\frac{(R^s_{ox/red})_1}{(R^s_{ox/red})_2} = \frac{\left(1 + \dfrac{k_1 + k_D}{(k_{h\nu})_1}\right)}{\left(1 + \dfrac{k_1 + k_D}{(k_{h\nu})_2}\right)} = \frac{(k_{h\nu})_2[(k_{h\nu})_1 + k_1 + k_D]}{(k_{h\nu})_1[(k_{h\nu})_2 + k_1 + k_D]} \quad (1)$$

where $(R^s_{ox/red})_x$ is the ratio between the integrated intensities of the peaks corresponding to the oxidized and reduced species at incident laser flux x. For this expression to be useful, an estimate of the rate constant $k_{h\nu}$ is required. It can be assumed that in these experiments the rate constant for Ru excitation can be written in terms of the Ru-moiety extinction coefficient and the incident photon density. For Ru(lys72)cyt.c, the extinction coefficient for the Ru group at 406 nm is about 6800 M^{-1} cm^{-1}, which corresponds to $\epsilon^t_{Ru} = 2 \times 10^{14}$ M^{-1} s^{-1}. The rate constants for Ru excitation are simply these ϵ^t_{Ru} values multiplied by the initial photon density $[h\nu_0]$. By using these values for $k_{h\nu}$ and the above relationships, the transient resonance Raman data can be analyzed.

The TRRR spectra can be treated by assuming that at $t = 0$, the system is entirely in the Ru^{2+}*/Fe^{3+} cyt.c state and that $k_{h\nu} = 0$ from $t = 0$ forward. With these approximations, the ratio of oxidized cytochrome *c* to reduced cytochrome *c* at any time subsequent to the pump beam ($t = 0$) can be written

$$\frac{ox}{red} = \frac{\left[(1 - e^{-k_2 t}) + \dfrac{k_D - k_2}{k_1}(1 - e^{-(k_D + k_1)t}) + \dfrac{k_D + k_1 - k_2}{k_1} e^{-k_2 t}\right]}{[e^{-k_2 t} - e^{-(k_D + k_1)t}]} \quad (2)$$

where the rate constants are defined as above (Figure 7). As in the steady-state case, the difference in the scattering cross-sections for the reduced and oxidized species can be accounted for by analyzing the ratios of values at different time points.

(1) *Ru(lys72) Cytochrome c*. The spectral data from the Ru(lys72)cyt.c experiments reveal that the behavior of this derivative under the current experimental conditions differs significantly from that predicted by the mechanism in Figure 7. The TRRR results show a fairly rapid rise in the fraction of the reduced species, followed by a very long recovery phase. The maximum reduction is observed at 100 ns to 1 μs, and significant (~10%) pump-induced reduction remains for as long as 11.4 ms after the pump.

The TRR results also disagree with predictions based upon Figure 7 and Table 5. The Ru(lys72)cyt.c exhibits a nearly constant high degree of photoinduced reduction over a range of 100%−25% of the maximum incident laser flux. Decreasing the flux to 12.5% of maximum results in complete loss of the reduced contribution within the signal-to-noise ratio of the spectrum. These data cannot be fit with eq 2 or the published rate constants determined by transient absorbance spectroscopy (Durham et al., 1989). Previous transient absorbance measurements (Durham et al., 1989) made upon the Ru(lys72) derivative show a fast rise time for the reduced species, followed by nearly as rapid a decay. The maximum fraction of reduced species was observed at ~75 ns, and the system returned to its original state within a $\Delta t = 400$ ns. The values of k_1, k_2, and k_D in Table 5 fit this transient absorbance data (Durham et al., 1989).

The discrepancies in the Ru(lys72)cyt.c behavior observed Durham et al. (1989) and that reported here can be explained in terms of the differences between the two experimental protocols. In the transient absorbance experiments, the Ru was pumped with a fairly low intensity, 450 nm source, and only a small net amount of reduced heme species is generated. In contrast, the lower sensitivity of the resonance Raman experiments required that a significant population of reduced heme be generated, and thus relatively high excitation intensities were necessary. Excitation of the Ru(lys72)cyt.c samples with 450 nm pulses did not generate reliably quantifiable populations of ferrous heme, even at the earliest Δt values. Therefore, the TRRR experiments were carried out using high-intensity 355 nm pulses. This protocol is distinct from those employed in the earlier transient absorption studies in two important ways: with an intense 355 nm pump pulse, (1) the Ru group CT state is not directly photoexcited and thus the Ru* must internally relax to the ET-active excited state(s), and (2) other chromophores within the sample may be photoexcited.

We propose that the ET behavior of Ru(lys72)cyt.c follows the mechanism depicted in Figure 8. The long relaxation time associated with the reduced heme can be explained in terms of a photoexcited sacrificial donor (SAC) in proximity to the Ru group. Exposure of the sample to the intense 355 nm pump beam excites both the Ru and the SAC. The excited SAC* competes with the back-transfer process to produce a new, much more stable species, Ru^{2+}−Fe^{2+}−cyt.c.

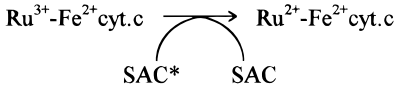

For this pathway to dominate the branching point, k_2' must be at least an order of magnitude larger than k_2 ($k_2' \geq 24 \times 10^7$ s^{-1}), and the concentration of SAC* must be significant.

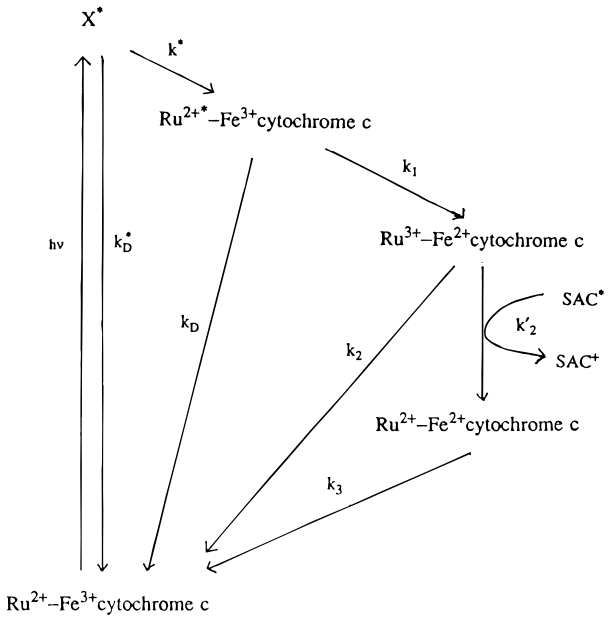

FIGURE 8: Proposed reaction scheme for photoinduced ET in the resonance Raman experiments. SAC* and SAC^+ refer to the photoexcited and oxidized sacrificial donors, respectively.

The step mediated by k_2' is an ET step, and thus, the magnitude of k_2' is exponentially dependent on the distance between the Ru group and the SAC*. The rapidity with which this step must occur rules out diffusion as a mechanism for bringing the donor and acceptor together. The SAC* is therefore likely to be part of the protein. Candidates for SAC* include the aromatic amino acids Trp, Tyr, and Phe, which absorb in the 350 nm region of the spectrum. In view of the intensity of the pump pulses, even low quantum yield excitations may in fact produce appreciable populations of SAC* from these species. Examination of the crystal structure of horse heart cytochrome *c* reveals that there are four aromatic amino acids, Trp 59, Tyr 74, Phe 82, and Tyr 67, in close proximity to Lys 72 (Bushnell et al., 1990).

It is important to recall that the experiments described here monitor only the oxidation state of the heme center. Thus, the $Ru^{3+}-Fe^{2+}$ cyt.c and $Ru^{2+}-Fe^{2+}$ cyt.c species contribute indistinguishably to the resonance Raman spectrum of the ferrous heme. The reaction that restores the ferrous heme to its initial ferric redox state,

$$Ru^{2+}-Fe^{2+}\text{cyt.c} \xrightarrow{k_3} Ru^{2+}-Fe^{3+}\text{cyt.c}$$

is expected to be slow even under aerobic conditions because there are no suitable electron donors near the heme group. Under our experimental conditions, this reaction replaces

$$Ru^{3+}-Fe^{2+}\text{cyt.c} \xrightarrow{k_2} Ru^{2+}-Fe^{3+}\text{cyt.c}$$

as the rate-limiting step in cytochrome *c* reoxidation and controls the long-time (>200 ns) behavior of the ET system. A value of $k_3 = 20-100\ s^{-1}$, when used in eq 2 to replace k_2, yields kinetic predictions that closely reflect the time-dependent behavior evident in the experimental data.

(2) *Ru(cys102) Cytochrome c.* The photoinduced ET kinetics of cys-102 yeast cytochrome *c* are not as well characterized as those of lys-72 horse heart cytochrome *c*. The only direct transient absorption study of this protein (Geren et al., 1991) was primarily concerned with the subsequent ET from photoreduced Ru(cys102)cyt.c to other redox proteins and thus reported only a lower limit for the initial photoinduced ET rate ($>10^5\ s^{-1}$). The current time-resolved resonance Raman data reveal much faster ET kinetics under our experimental conditions. Measurable reduced heme was found only at the earliest time point, 10−40 ns, after the pump. No evidence of photoinduced reduction was observed at 75 ns or later. Clearly, there is not enough information in this single data point to perform a kinetic analysis. However, it is clear that no long-lived reduced cytochrome *c* is formed. Thus, we conclude that there is no participation in this system of a sacrificial donor analogous to that observed in the Ru(lys72)cyt.c experiments. The explanation for this absence is 2-fold. First, examination of the crystal structure of yeast cytochrome *c* reveals that there are no aromatic amino acids close to the Ru-labeled cysteine 102 (Louie et al., 1988). Also, the excitation pulses in these experiments were at 450 nm, in resonance with the transition to the $Ru^{2+}*-Fe^{3+}$cyt.c charge-transfer state (Cherry & Henderson, 1984). It was not possible to obtain time-dependent measurements using 355 nm pump pulses in this system, as the fluorescence background overwhelms the Raman signal using this pump wavelength.

The behavior of the Ru(cys102)cyt.c in response to increasing laser flux also is at least qualitatively consistent with the simpler photocycle in Figure 7. The relative amount of reduced heme species decreases as the incident laser flux is decreased. No saturation is observed. It appears in our Raman experiments that the sum ($k_1 + k_D$) in the cysteine-modified protein system is slightly larger than that in the lysine-modified protein system. However, time-resolved luminescence studies by F. Millett and L. Durham (unpublished) have established an intramolecular rate constant for forward ET of less than $1 \times 10^6\ s^{-1}$. This rate is more consistent with the smaller ΔG^* and larger distances of photoinduced ET in the Ru(cys102)cyt.c relative to Ru(lys72)cyt.c (Geren et al., 1991). The ET kinetics observed in the present study are clearly much faster. In order to resolve this discrepancy, control experiments were conducted that revealed no observable ET occurring within 10 ns in native yeast cytochrome *c* under solution and excitation conditions similar to those described for Figure 4 (data not shown). These results ensure that the Ru−polypyridine moieties are, in fact, acting as the donors in the ET process evident in the TRR spectra. We speculate that the higher concentrations of Ru cyt.c required for TRR studies (∼100 μM vs ∼3 μM for luminescence studies) produce protein aggregates that exhibit rapid intermolecular ET.

Structural Dynamics Accompanying Photoinduced Electron Transfer. The mechanisms by which protein structure modulates ET rates is a subject of continuing debate. A host of physical investigations have revealed the importance of free energy, donor−acceptor distance, reorganizational energies, and electron tunneling pathways in controlling the net rate of ET in these complex systems [see the recent minireviews in J. Bioenerg. Biomembr. (1995) *27*, 261, for excellent summaries of the current status of the field]. All of these parameters depend, in turn, on both the local environments of the donor/acceptor and the longer-range structure of their protein hosts. In particular, it has become increasingly evident that the structural dynamics of the redox active sites and the intervening protein can profoundly affect long-range electronic coupling and electron tunneling path-

ways (Wuttke et al., 1992; Langen et al., 1995; Stuchebrukov & Marcus, 1995; Siddharth & Marcus, 1990; Onuchi & Beretan, 1990; Curry et al., 1995). Recent experimental studies of photoinitiated ET in Ru-derivatized proteins (principally cytochromes *c*) have been very useful in addressing the complexity of protein-mediated ET (Bjerrum et al., 1995, and references therein; Winkler et al., 1982; Pan et al., 1988). However, while much insight has been gained concerning the effects of equilibrium structures on net ET rates, little or no experimental evidence exists concerning the evolution of the system on the time scales of the structural dynamics accompanying ET. The data obtained in this study address this issue and provide important insights into the structural dynamics of the heme and its environment during ET in cytochromes.

The energetics of structural reorganization can be phenomenlogically expressed as a nuclear reorganizational energy, λ, which, in turn, can be viewed as the sum of two contributions (Marcus & Sutin, 1985; Marcus, 1956, 1964, 1965). The inner-sphere reorganization (λ_i) involves the nuclei of the immediate coordination shells of the redox centers. The outer-sphere reorganization (λ_o) occurs in the "solvent" outside of the inner shell. The nuclear reorganization energy λ has been fairly well studied in the redox reactions of cytochrome *c* (Marcus & Sutin, 1985; Gupta, 1973; Brunschwig et al., 1986; Bowler et al., 1989; Therien et al., 1990; Churg et al., 1983; Meade et al., 1989). Though the actual calculated and measured values vary, all of the studies indicate that the total nuclear reorganization energy in cytochrome *c* systems is composed of a large outer-sphere component and a relatively small inner-sphere component. The contribution of the outer sphere is estimated to exceed that of the inner sphere by a factor of 4−5. In heme-containing proteins, λ_i most directly corresponds to the heme and its direct linkages to the protein, and λ_o reflects the response of the surrounding protein and the aqueous solvent. The data obtained in this study probe only the structural dynamics directly tied to the heme active site.

Resonance Raman spectroscopy is an effective probe of nuclear reorganization at and near the heme. Over the past two decades, the normal modes of hemes have been well characterized, and their behaviors as a function of heme geometry and structural dynamics have been extensively studied in a wide variety of heme proteins [see Rousseau and Friedman (1988) and Findsen and Ondrias (1990) for reviews]. Fortunately, the strongest band in the heme resonance Raman spectrum, ν_4, is quite responsive to fluctuations in the macrocycle π^* electron density that may be engendered by structural changes at or near the heme. Crystal structures of equilibrium ferrous and ferric yeast cytochromes *c* show no large-scale differences in tertiary protein structure but do reveal small differences in the heme local environment (Louie et al., 1988). Likely candidates for ET-sensitive heme structural components include His and Met axial ligation, thioether linkages to the protein, equilibrium between planar and nonplanar heme conformations, and nonbonded interactions of propionate side chains. Changes in these degrees of freedom are expected to sterically and/or electronically alter heme π^* density and thereby be reflected in changes in the position and/or width of ν_4 and other heme modes.

The general tertiary structure and specific heme environments of soluble cytochromes *c* are highly conserved (Dickerson, 1972). Our data are quite consistent with previous Raman-difference and more recent molecular modeling studies by Shelnutt and co-workers (1981; Hobbs & Shelnutt, 1995) that revealed only small structural differences between the equilibrium hemes in the yeast and horse heart cytochromes. Nonetheless, the ET kinetics of the two proteins differ significantly. For instance, yeast cytochrome *c* exhibits a self-exchange rate an order of magnitude slower than that of horse heart cytochrome *c* (Gupta, 1973). The insensitivity of these and other kinetic differences to ionic strength and pH (Gupta, 1973) makes it unlikely that they result from variations in protein complex formation and/or heme exposure to the solvent. Thus, it is likely that nuclear reorganization processes and structural dynamics play significant roles in determining ET rates in these systems.

There is a precedent for the expectation that structural evolution occurring at the donor/acceptor sites may influence the net ET dynamics of cytochromes. An analogous situation occurs in the ligation dynamics of hemoglobins where the structural rearrangements of the immediate heme environment and of more global protein configurations have been demonstrated to be of pivotal importance for molecular function. The photolysis and religation dynamics of hemoglobins and myoglobins have been carefully studied using TRRS and can be divided into two distinct phases: (1) a rapid (<10 ns) relaxation of the heme itself from a planar, low-spin species to a domed, high-spin geometry and the creation of a metastable heme pocket configuration and (2) the evolution of the heme pocket to a new equilibrium configuration on a much slower time scale (>1 μs) (Rousseau & Friedman, 1988; Findsen & Ondrias, 1990; Friedman et al., 1982; Terner et al., 1981; Dasgupta et al., 1985; Scott & Friedman, 1984; Findsen et al., 1985, 1988; Carson et al., 1987; Schneebeck et al., 1993). The time scale and dependence on solvent viscosity of the second phase strongly suggest that it is predicated on concerted motions of global protein domains directly reflected in the heme pocket geometry. The rate of evolution of heme pocket structure can be correlated to the functional distinctions among various hemoglobin tertiary and quaternary structures (Rousseau & Friedman, 1988; Findsen & Ondrias, 1990; Scott & Friedman, 1984; Findsen et al., 1985).

The principle goal of this investigation was to determine the time scales involved in the structural dynamics of the heme and its environment subsequent to photoinduced ET in cytochromes *c*. By analogy to ligation dynamics, the structural evolution of the cytochrome *c* heme site subsequent to ET might be expected to exhibit two temporally distinct processes:

(i) a rapid response of the heme and its immediate environment to the ET event (λ_i), and

(ii) a slower, more global reorganization of protein residues more removed from the heme (λ_o).

Time-resolved spectra of both cytochromes show no evidence for the slower phase. The positions and line shapes of ν_4 (and other high-frequency modes) are indistinguishable from those of the equilibrium hemes within 50 ns of photoinduced ET. Thus we must conclude that no long-lived metastable geometry is created at the heme during ET in either protein investigated. This strongly suggests that the protein−heme interactions of the local heme pocket respond very rapidly to the ET-induced structural changes of the heme itself (most notable the small changes in the

heme core-size and iron−ligand bond lengths upon iron reduction). In particular, any distortions in the heme−axial ligand geometry would be expected to be reflected in a non-equilibrium position for ν_4 of the newly created ferrous heme. It appears that, in contrast to hemoglobins, the local protein environment offers little or no energetic barrier to heme structural reorganization in cytochromes. Moreover, any subsequent changes in protein tertiary structures occurring in regions away from the active site do not perturb the immediate heme environment.

The transient resonance Raman studies probe structural dynamics on faster time scales than the time-resolved protocols. In fact, the power dependence of the positions and line widths of heme modes reflect relaxation processes that occur more rapidly than the temporal width of the excitation pulses but slower than the average Δt between photon−molecule interactions. Under our experimental conditions, relaxations occurring in less than 1−2 ns would not be readily observed.[2] We conclude that structural dynamics associated with λ_i occur on time scales that are competitive with the ET event. In this regard, the transient spectra in Figures 3 and 4 reveal potentially important protein-specific differences in ET structural dynamics. In contrast to the previously reported (Simpson et al., 1995) power dependence in the position and line width of the ν_4 ferrous band during ET in Ru(cys102) yeast cytochrome *c*, the behavior of this line for Ru(lys72) horse heart cytochrome *c* is independent of laser flux in the transient experiments. This result indicates that the structural relaxation of the heme itself is more rapid in the horse heart protein ($\tau_{1/2}$ < 1−2 ns) than in the yeast. In view of the insensitivity of the equilibrium heme environments to ruthenation, we assume that the differences in the early time dynamics arise from species specific variations in protein structure and not differences in ruthenation site.

SUMMARY AND CONCLUSIONS

Our investigations represent the first comprehensive use of transient and time-resolved resonance Raman techniques for the study of photoinduced ET in cytochromes. While these initial studies generate many questions that must be further addressed, they also lead to the following conclusions:

(1) Resonance Raman protocols can be effectively employed to trace both the kinetics of ET and its associated structural dynamics in protein systems. The requirements for higher concentrations and excitation fluences in the Raman experiments can affect the overall ET process by creating additional photoactive species and/or allowing for intermolecular ET. Therefore, care must be exercised in directly comparing the results of time-resolved resonance Raman and absorption/fluorescence investigations.

(2) The fast inner-sphere reorganizational processes of the heme and its immediate environment dominate the TRRS results. These dynamics are very rapid relative to the phenomenological ET kinetics of cytochromes *c*. The heme and its local environment evolve to their equilibrium (ferrous) structures in <10 ns with no evidence for the existence of metastable heme pocket geometries.

(3) Species-specific differences are observed in the rate of this rapid structural response to ET. These are evident only at higher excitation fluences and thus reflect heme dynamics occurring on nanosecond or faster time scales.

APPENDIX 1

Details of the Kinetic Analysis

Given the reaction scheme in Figure 7, the following rate equations can be written:

$$\frac{d[Ru^{2+}-Fe^{3+}cyt.c]}{dt} = -k_{h\nu}[Ru^{2+}-Fe^{3+}cyt.c] + k_D[Ru^{2+}*-Fe^{3+}cyt.c] + k_2[Ru^{3+}-Fe^{2+}cyt.c] \quad (A1)$$

$$\frac{d[Ru^{2+}*-Fe^{3+}cyt.c]}{dt} = -(k_1 + k_D)[Ru^{2+}*-Fe^{3+}cyt.c] + k_{h\nu}[Ru^{2+}-Fe^{3+}cyt.c] \quad (A2)$$

$$\frac{d[Ru^{3+}-Fe^{2+}cyt.c]}{dt} = k_1[Ru^{2+}*-Fe^{3+}cyt.c] - k_2[Ru^{3+}-Fe^{2+}cyt.c] \quad (A3)$$

The resonance Raman data are examined in terms of these rate expressions and the published kinetic data.

The TRR technique measures the steady-state populations of the reactants, products, and intermediates of the photo-initiated reaction as a function of the average time between excitations. Thus steady-state approximations can be applied to the above rate equations. Subsequent rearrangement yields

$$\frac{ox}{red} = \frac{k_2}{k_1}\left(1 + \frac{k_1 + k_D}{k_{h\nu}}\right) \quad (A4)$$

where the observables are the relative populations of the heme redox states. In the experiments here, $[Ru^{2+}-Fe^{3+}$-cyt.c] and $[Ru^{2+}*-Fe^{3+}cyt.c]$ are assumed to be indistinguishable. For this reason

$$[ox] = [Ru^{2+}-Fe^{3+}cyy.c] + [Ru^{2+}*-Fe^{3+}cyt.c] \quad (A5)$$

$$[red] = [Ru^{3+}-Fe^{2+}cyt.c] \quad (A6)$$

The scattering from the oxidized Fe cytochrome *c* relative to the reduced Fe cytochrome *c* is given by

[2] The transient Raman data are also consistent with rapid (<10 ns) structural relaxation at the heme subsequent to ET. The results can be analyzed to reveal species-specific characteristics and estimates of the upper limits for relaxation lifetimes. In these experiments, two photons are required to interact with a given molecule for a reduced ν_4 band to be observed: one to initiate the ET reaction and one to probe the intermediates and products via Raman scattering. It is known that the reoxidation of the heme occurs with a >10 ns lifetime (Geren et al., 1991; Durham et al., 1989). Therefore, each molecule can only be photoreduced once in a given laser pulse. The incident laser flux determines the average time interval between the "pump" and "probe" photons within a given laser pulse. If the initial relaxation is rapid on the timescale of this incident laser pulse (i.e., <10 ns), then the distribution of electronic and structural states in the population that is probed by Raman spectroscopy is expected to be sensitive to the incident laser flux. At low flux, the molecules have, on average, sufficient time to relax prior to being probed and thus yield vibrational bands indicative of the equilibrium reduced species. At higher laser fluence, the relaxing molecules are, on average, probed before they can relax, and the spectrum reflects the net contributions from hemes in various stages of relaxation. If the vibrational properties of the transient and relaxed species vary, then the position and width of the net Raman bands observed within an ~10 ns pulse will be quite sensitive to small differences in the time between "pump" and "probe" photons (i.e., to photon flux).

$$R^{s}_{ox/red} = \frac{I^{s}_{[ox]}}{I^{s}_{[red]}} = \left[\frac{k_2}{k_1}\left(1 + \frac{k_1 + k_D}{k_{h\nu}}\right)\right]\frac{\sigma^{s}_{ox}}{\sigma^{s}_{red}} \qquad \text{(A7)}$$

The cross-sections for Raman scattering from reduced (σ^{s}_{red}) and oxidized (σ^{s}_{ox}) hemes are not necessarily equal, so ($\sigma^{s}_{ox}/\sigma^{s}_{red}$) $\neq$ 1. In order to bypass the requirement for explicit knowledge of these cross-sections, the transient resonance data are analyzed in ratio form.

$$\frac{(R^{s}_{ox/red})_1}{(R^{s}_{ox/red})_2} = \frac{\left(1 + \frac{k_1 + k_D}{(k_{h\nu})_1}\right)}{\left(1 + \frac{k_1 + k_D}{(k_{h\nu})_2}\right)} = \frac{(k_{h\nu})_2[(k_{h\nu})_1 + k_1 + k_D]}{(k_{h\nu})_1[(k_{h\nu})_2 + k_1 + k_D]} \qquad \text{(A8)}$$

For this expression to be useful, an estimate of the rate constant $k_{h\nu}$ is required.

The forward rate constant $k_{h\nu}$ is pseudo-first-order. The actual reaction involved is

$$\mathrm{Ru} + h\nu \xrightarrow{k'} \mathrm{Ru}^* \qquad \text{(A9)}$$

This is a second-order reaction dependent upon both the concentration of Ru and the intensity of the incident beam. Under typical experimental conditions, there are on the order of 10^{14} photons/pulse (illumination volume). This value is an estimate based on 1 mW laser intensity at the sample at 406 nm and 15 Hz. Assuming an illuminated volume of 8 $\times$ 10^{-4} cm^3, the photon "concentration" becomes approximately 0.3 mM. The relatively low concentration of Ru and its small extinction coefficient [$\epsilon_{Ru(lys72)cyt.c} = 6800$ M^{-1} cm^{-1}; $\epsilon_{Ru(cys102)cyt.c} = 6250$ M^{-1} cm^{-1}] suggest that the assumption of $[h\nu] = [h\nu]_0$ is valid.

Implementation of this assumption leads to the pseudo-first-order reaction

$$\mathrm{Ru} \xrightarrow{k_{h\nu}} \mathrm{Ru}^* \qquad \text{(A10)}$$

where $k_{h\nu} = k'[h\nu]_0$. The k' is the rate constant that describes the coupling efficiency in time of the reaction between Ru and the photon. This rate constant can be written in terms of the traditional extinction coefficient of the Ru group as

$$k' = \epsilon^{t}_{Ru} = \epsilon^{d}_{Ru}c \qquad \text{(A11)}$$

where ϵ^{d}_{Ru} is the traditional extinction coefficient of Ru relative to the path length of the sample, ϵ^{t}_{Ru} is the extinction coefficient of Ru relative to time, and c is the speed of light. For Ru(lys72)cyt.c, the extinction coefficient for the Ru group at 406 nm is about 6800 M^{-1} cm^{-1}. This corresponds to $\epsilon^{t}_{Ru} = 2 \times 10^{14}$ M^{-1} s^{-1}. The extinction coefficient for the Ru group in Ru(cys102)cyt.c is slightly smaller (6250 M^{-1} cm^{-1}), yielding $\epsilon^{t}_{Ru} = 1.9 \times 10^{14}$ M^{-1} s^{-1}. The rate constants for Ru excitation are simply these ϵ^{t}_{Ru} values multiplied by the initial photon density $[h\nu]_0$. Transient resonance Raman data can be analyzed by using these values for $k_{h\nu}$ and the relationships in eqs A8 and A11.

The time-resolved resonance Raman spectra also can be treated in terms of the rate expressions A1, A2, and A3. It is assumed that at $t = 0$, the system is entirely in the Ru^{2+}*$-Fe^{3+}$cyt.c state and that $k_{h\nu} = 0$ from $t = 0$ forward. With these approximations in mind, the ratio of oxidized cytochrome *c* to reduced cytochrome *c* at any time subsequent to the pump beam can be written

$$\frac{\mathrm{ox}}{\mathrm{red}} = \frac{\left[(1 - e^{-k_2 t}) + \frac{k_D - k_2}{k_1}(1 - e^{-(k_D + k_1)t}) + \frac{k_D + k_1 - k_2}{k_1}e^{-k_2 t}\right]}{[e^{-k_2 t} - e^{-(k_D + k_1)t}]} \qquad \text{(A12)}$$

where the rate constants are defined as above (Figure 7). As in the steady-state case, the difference in the scattering cross-sections for the reduced and oxidized species can be accounted for by analyzing the ratios of values at different time points.

In the experiments on the lysine-labeled protein, the probe pulses generated a small amount of reduced heme. In order to correct the time-resolved spectra for this contribution from the probe initiated ET, the following was used:

$$\text{corrected reduced fraction} = \left[\frac{R_m}{R_m + O_m} - \frac{R_p}{R_p - O_p}\right]\left[\frac{1}{1 - \frac{R_p}{R_p + O_p}}\right]$$

The subscripts m and p denote the measured and probe-only values, respectively. R is the integrated intensity of the reduced species, and O indicates the integrated intensity of the oxidized species (see Table 3).

APPENDIX 2

Details of the Spectral Fitting Analysis

Spectra were fit as follows. All spectra were decomposed into Lorentzian line shapes with either a quadratic or a linear base line function. For the high, sloping backgrounds found in the time-resolved spectra associated with the Ru(cys102)-cyt.c sample, the background was fit in two steps. First, a quadratic function was fit to the background. This curvature was subtracted from the data, which were then fit with a linear base line. For the transient and time-resolved measurements of ν_4, the widths and positions of the other peaks in the spectra were fixed according to equilibrium values. The fit of the ν_4 region was allowed to converge without fixing any parameters, except as noted in Tables 3 and 4. Any fixed widths for the ν_4 bands were set to the values measured in spectra taken of equilibrium species.

A curvefitting program was written based upon the Levenberg−Marquardt nonlinear least-squares method (Simpson, 1994) that has a number of specific advantages over commercially available packages for fitting data of the type obtained in this study: (1) The step size taken during minimization can be varied as needed, (2) the minimization process is monitored at each step, and (3) the total intensities of the signal and background are irrelevant. These features provide more control over the fitting process, thereby allowing the accurate fitting of low-intensity data on low or

high backgrounds and significantly reducing fitting errors such as convergence to local minima.

This routine was extensively tested on both real and simulated data in order to evaluate its limitations. The sensitivity of fit results to initial parameter guesses (peak height, width, and position) was explored. In addition, simulated spectra with a variety of signal-to-noise ratios, peak separations, and peak relative intensities were fit. It was determined that the present data are well within the program's ability to correctly resolve two overlapping components. Additional details concerning data analysis controls are available as supporting information.

SUPPORTING INFORMATION AVAILABLE

Details on data collection and analysis (2 pages). Ordering information is given on any current masthead page.

REFERENCES

Beratan, D. N., Betts, J. N., & Onuchic, J. N. (1991) *Science 252*, 1285.

Beratan, D. N., Onuchic, J. N., Winkler, J. R., & Gray, H. B. (1992) *Science 258*, 1740.

Bjerrum, M. J., Casimiro, D. R., Chang, I.-J., Di Bilio, A. J., Gray, H. B., Hill, M. G., Langen, R., Mines, G. A., Skov, L. K., Winkler, J. R., & Wuttke, D. S. (1995) *J. Bioenerg. Biomembr. 27*, 295.

Bowler, B. E., Meade, T. J., Mayo, S. L., Richards, J. H., & Gray, H. B. (1989) *J. Am. Chem. Soc. 111*, 8757.

Brunschwig, B. S., Ehrenson, S., & Sutin, N. (1986) *J. Phys. Chem. 90*, 3657.

Bushnell, G. W., Louie, G. V., & Brayer, G. D. (1990) *J. Mol. Biol. 214*, 585.

Carson, S. D., Wells, C. A., Findsen, E. W., Friedman, J. M., & Ondrias, M. R. (1987) *J. Biol. Chem. 262*, 3044.

Cherry, W. R., & Henderson, L. J., Jr. (1984) *Inorg. Chem. 23*, 983.

Churg, A. K., Weiss, R. M., Warshel, A., & Takano, T. (1983) *J. Phys. Chem. 87*, 1683.

Curry, W. B., Grabe, M. D., Kurnikov, I. V., Skourtis, S. S., Beratan, D. N., Regan, J. J., Aquino, A. J. A., Beroza, P., & Onuchic, J. N. (1995) *J. Bioenerg. Biomembr. 27*, 285.

Cusanovich, M. A. (1991) *Photochem. Photobiol. 53*, 845.

Dasgupta, J., Spiro, T. G., Johnson, C. K., Dalickas, G. A., & Hochstrasser, R. M. (1985) *Biochemistry 24*, 5295.

Dickerson, R. E. (1972) *Sci. Am.*, 58−72.

Durham, B., Pan, L. P., Long, J., & Millett, F. (1989) *Biochemistry 28*, 8659.

Ferguson-Miller, S., Brautigan, D. L., & Margoliash, E. (1977) in *The Porphyrins* (Dolphin, D., Ed.) Vol. 3, pp 149−240, Academic Press, New York.

Findsen, E. W., & Ondrias, M. R. (1988) *Appl. Spectrosc. 42*, 445.

Findsen, E. W., & Ondrias, M. R. (1990) *Photochem. Photobiol. 51*, 741.

Findsen, E. W., Friedman, J. M., Ondrias, M. R., & Simon, S. R. (1985) *Science 229*, 661.

Findsen, E. W., Friedman, J. M., & Ondrias, M. R. (1988) *Biochemistry 27*, 8719.

Friedman, J. M., Rousseau, D. L., Ondrias, M. R., & Stepnoski, R. A. (1982) *Science 278*, 1244.

Geren, L., Hahm, S., Durham, B., & Millett, F. (1991) *Biochemistry 30*, 9450.

Geren, L. M., Beasley, J. R., Fines, B. R., Saunders, A. J., Hibdon, S., Pielak, G. J., Durham, B., & Millett, F. (1995) *J. Biol. Chem. 270*, 2466.

Gupta, R. K. (1973) *Biochim. Biophys. Acta 292*, 291.

Hobbs, J. D., & Shelnutt, J. A. (1995) *J. Protein Chem. 14*, 19.

Louie, G. V., Hutcheon, W. L. B., & Brayer, G. D. (1988) *J. Mol. Biol. 199*, 295.

Langen, R., Chang, I.-J., Germanas, J. P., Richards, J. H., Winkler, J. R., & Gray, H. B. (1995) *Science 268*, 1733.

Marcus, R. A. (1956) *J. Chem. Phys. 24*, 966.

Marcus, R. A. (1964) *Annu. Rev. Phys. Chem. 15*, 135.

Marcus, R. A. (1965) *J. Chem. Phys. 43*, 679.

Marcus, R. A., & Sutin, N. (1985) *Biochim. Biophys. Acta 811*, 265.

McLendon, G. (1988) *Acc. Chem. Res. 21*, 160.

Meade, T. J., Gray, H. B., & Winkler, J. R. (1989) *J. Am. Chem. Soc. 111*, 4353.

Moser, C. C., Page, C. C., Farid, R., & Dutton, P. L. (1995) *J. Bioenerg. Biomembr. 27*, 263.

Onuchic, J. N., & Beratan, D. N. (1990) *J. Chem. Phys. 92*, 722.

Pan, L. P., Durham, B., Wolinska, J., & Millett, F. (1988) *Biochem. 27*, 7180.

Rousseau, D. L., & Friedman, J. M. (1988) in *Biological Applications of Raman Spectroscopy* (Spiro, T. G., Ed.) Vol. 3, pp 133, Wiley, New York.

Schneebeck, M. C., Vigil, L. E., Friedman, J. M., Chavez, M. D., & Ondrias, M. R. (1993) *Biochem. 32*, 1318.

Scott, T. W., & Friedman, J. M. (1984) *J. Am. Chem. Soc. 106*, 5677.

Shelnutt, J. A., Rousseau, D. L., Dethmers, J. K., & Margoliash, E. (1981) *Biochemistry 20*, 6485.

Siddharth, P., & Marcus, R. A. (1990) *J. Phys. Chem. 94*, 8430.

Simpson, M. C. (1994) Ph.D. Dissertation, University of New Mexico, School of Medicine, Albuquerque, New Mexico.

Simpson, M. C., Millett, F., Fan, B., & Ondrias, M. R. (1995) *J. Am. Chem. Soc. 117*, 3296.

Stuchebrukov, A. A., & Marcus, R. A. (1995) *J. Phys. Chem. 99*, 7581.

Terner, J., Stang, J. P., Spiro, T. G., Nagumo, M., Nicol, M. S., & El-Sayed, M. A. (1981) *Proc. Natl. Acad. Sci. U.S.A. 78*, 1313.

Therien, M. J., Selman, M., & Gray, H. B. (1990) *J. Am. Chem. Soc. 112*, 2420.

Winkler, J. T., Nocera, D. G., Yocum, K. M., Bordignan, E., & Gray, H. B. (1982) *J. Am. Chem. Soc. 104*, 5798.

Winkler, J. R., & Gray, H. B. (1992) *Chem. Rev. 92*, 369.

Wuttke, D. S., Bjerrum, M. J., Winkler, J. R., & Gray, H. B. (1992) *Science 256*, 1007.

BI960253Y